Paper

Transmission Measurement of the Absolute CMA; Simulation and Experiments

Adel Alkafri,[a] Y. Ichikawa,[a] R. Shimizu,[b] and K. Goto[c,*]
[a]*Nagoya Institute of Technology (NIT), Gokiso-cho, Showa-ku, Nagoya 466-8555*
[b]*Osaka Institute of Technology (OIT), Kitayama 1-79-1, Hirakata 573-0196*
[c]*Advanced Industrial Science and Technology (AIST), 2266-98 Shimoshidami, Moriyama-ku, Nagoya 463-8560*
**gotou.keisuke@aist.go.jp*

(Received: October 17, 2006; Accepted: April 4, 2007)

We measured the transmission of the cylindrical mirror analyzer (CMA) by using a mini-electron gun consisting of a tungsten hairpin cathode set at the sample position. The electron beam current (i_{in}) entering the CMA was measured using a retractable Faraday cup and an electrometer. The electrons get through the CMA and finally the detected current (i_{out}) representing only a fraction of the input current was measured using another Faraday cup (normally used for detecting Auger electrons) and another electrometer. The ratio of the i_{out} to i_{in} gives the transmission of the CMA. Besides the experiment, we simulated the transmission characteristics, i.e., peak heights, position, and full width at half maximum, assuming thermionic emission and Gaussian peak shape. The simulation revealed characteristics that the experiments would not show explicitly. An optical transmission measurement was performed as well providing a good agreement with the results of the present electron beam measurements.

1. Introduction

Electron spectroscopy is now very popular particularly in surface analysis. Many manufacturers make their sophisticated equipment produced by many manufacturers, capable for Auger electron spectroscopy (AES) and X-ray photoelectron spectroscopy (XPS) are distributed widely and used commonly [1-3]. However, the spectra obtained contain some arbitrariness regarding the absolute intensity and energy position of the peaks measured. The activity within the ISO Technical Committee 201 (Surface Chemical Analysis) [4-6] and the Versailles project on advanced materials and standards - Surface Chemical Analysis (VAMAS-SCA) [7-9] are trying to introduce the use of the SI (International System of Units) in the field of Surface Chemical Analysis and electron spectroscopy. In the sense of the metrology, the analyzer shall be "calculable" and every term must be defined with "uncertainty" [10]. The terms must be referred to the SI standards; the energy of the spectra peak being determined by the standard voltage (10 V) and a precision voltage divider, detected electron current by a calibrated electrometer. Moreover the transmission and the instrumental contribution to the background in the spectra are also important terms for electron energy analyzers. We made a precision high voltage (10 kV) divider with 10 ppm of uncertainty and have been using an electrometer (Keithley 642 LN) with 2% of uncertainty [11]. A novel cylindrical mirror analyzer (CMA) for an absolute measurement in the AES has been developed in our laboratory with the aids of National Institute for Material Science (NIMS) [11-13] and example spectra of AES by this CMA are available from the COMPRO program in Surface Analysis Society of Japan (SASJ) [14]. Some scientists have used the spectra for their own works. The transmission of the CMA can be measured by putting a well-defined virtual source of electrons at the sample position, which actually simulates real measurements with an identical beam diameter of the source as the primary beam of about 50 m [15]. Experimental spectra include some unresolved and unidentified features due to the finite energy resolution of the analyzer used. The simulation can help to understand the details of the spectra.

2. Experimental

Figure 1(a) shows a scheme of the experimental set-up. A mini-electron gun, used as a virtual electron source, was set at the sample position, providing thermal electrons (through thermal emission) of primary energy from 1 eV to 3 keV. The limiter strictly confines the emission angle within a cone of 42.3±6° as shown in Fig. 1(b). The mini-electron gun consists of a ball-shaped cathode of point tungsten filament and Wehnelt electrode, an outer view of which is shown in Fig. 1(c). The center spot of Fig. 1(d) is the ball-shaped cathode (0.3 mm in diameter) set at the center of the Wehnelt electrode. The emission current (i_{in}) was measured with a retractable Faraday cup, FC_1, [Fig. 1(e)] and an electrometer. The stability of the emission was better than 1% for the Wehnelt bias of 0 V throughout the measurements. The detected current (i_{out}) was measured by another set of Faraday cup (FC_2) and an electrometer (Keithley 642 LN) normally used for detecting Auger electrons in AES. The ratio of i_{out} to i_{in} gives the transmission of the CMA. There are two meshes [Fig. 1(a)], covering over the entrance ($Mesh_1$) and exit ($Mesh_2$) slits in the inner cylindrical electrode. These meshes should deteriorate the characteristics of the CMA. The meshes were of 100 mesh woven with gold plated tungsten wire of 27 m in diameter. To examine the mesh-effect, we simply observed an image of the mesh by setting a fluorescent screen just behind the $Mesh_1$. The observed pattern is shown in Fig. 1(f). The meshes were coated with aquadag and soot of butane gas to reduce secondary electrons and scattered electrons, and farther to obtain a stable work function [15]. The CMA system was evacuated by a turbo molecular pump and sputter ion pump to low 10^{-5} Pa. The system was not baked for the convenience and to ensure the mechanical preciseness of the CMA-system.

3. Experimental results

3.1. Transmission

We measured the transmission of CMA to plot it as a function of the primary energy (E_p; primary acceleration voltage in a strict sense). The result is presented in Fig. 2 where the theoretical curve based on the first approximation is depicted with a solid line for cathode temperature

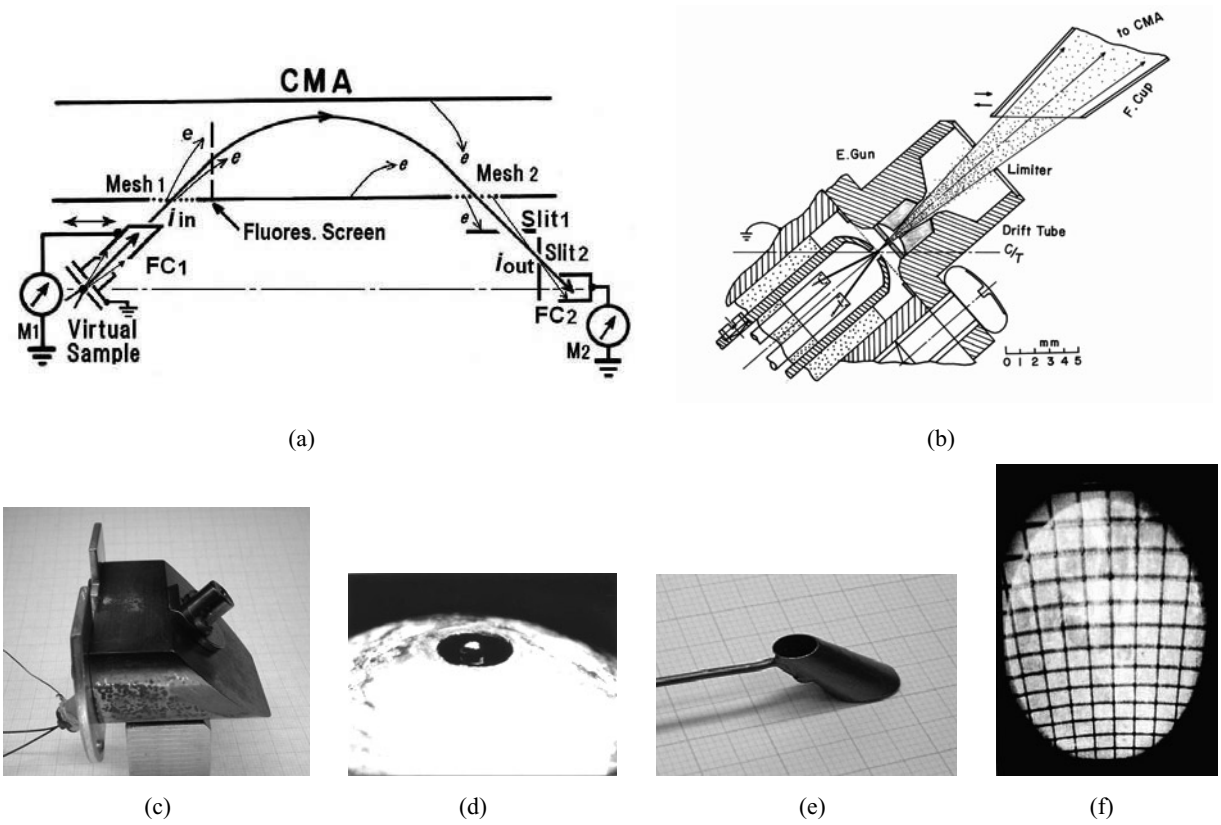

Fig. 1. Experiments: (a) Schematic experimental set up, (b) details of mini-electron gun, (c) photo of mini-electron gun, (d) ball cathode and Wehnelt, (e) mini-Faraday cup (FC1), (f) light of the cathode and the emission pattern of dear edge on the fluorescent screen; mesh being a photo-etched 25-mesh and 50 m only for the checking.

T=2043 K and $\Delta E/E$=0.25%. The broken line represents the ideal characteristics of the CMA with the energy window, attaining the break point, E_c=172 eV, where FWHM of the main peak of the emitted electrons becomes equal to the energy window of the CMA. Above E_c, where the energy window of CMA becomes wider than the FWHM of the main peak of emitted electrons, all the electrons of the main peak are detected, leading to the transmission being constant at ~31%. Since signal electrons pass through two meshes ($Mesh_1$ and $Mesh_2$) and the transmission of one mesh ($Mesh_1$) was estimated as 0.57 by optical transmission measurement, which was performed with halogen lamp and phototube in a similar set up as in the actual CMA, the net transmission should be estimated as $(0.57)^2$=0.32, which agrees with the experimental result (0.31), provided that the shade of the pattern like Fig. 1(f) having been randomized at the second mesh, $Mesh_2$. If the pattern of the $Mesh_1$ would completely overlaps on the $Mesh_2$, then the transmission of about 57%, but in other extreme, half of the value, i.e., about 29% could be resulted. As a whole, a moiré would occur. This result suggests that the optical transmission is a good measure to evaluate the transmission of signal electrons of energies higher than E_c. The experiment has revealed that the energy distribution of primary electrons provided by the present mini-electron gun is liable to being distorted for bias voltage of the Wehnelt electrode at lower E_ps. In the higher E_ps, the effects of the transmission characteristics of the CMA would be predominant. A typical example for the acceleration voltage V_p=5 V is shown in Fig. 3. The changes of the shape and peak position were significant. It is, therefore, crucial to set an appropriate operating condition of the mini-electron gun, particularly, for lower E_p. This experiment is continuing.

3.2. Simulation:

To examine the appropriate operating condition we performed a simple simulation for different temperatures T of thermionic emission electrons and the equivalent Gaussian energy distributions, which were assumed to be emitted for different values of energy resolution $\Delta E/E$ (CMA energy resolution function of "triangle"; 0.2, 0.25, 0.4, 0.6%, among which the energy resolution of 0.25% can be applied to our CMA [11]). The simulation consists of finding the total energy distribution (E_p=1 eV~5 keV) of CMA by calculating the convolution of $EN(E)$ characteristics with CMA energy resolution function. The convolution shall alter the energy position, spectral peak heights (intensity) and full width at half maximum (FWHM). The energy distribution of thermionic electrons was calculated using the formula reported by Young [16].

The results are depicted in Fig. 4 for the cathode temperature, 2043, 2300 and 2600 K, respectively, for the

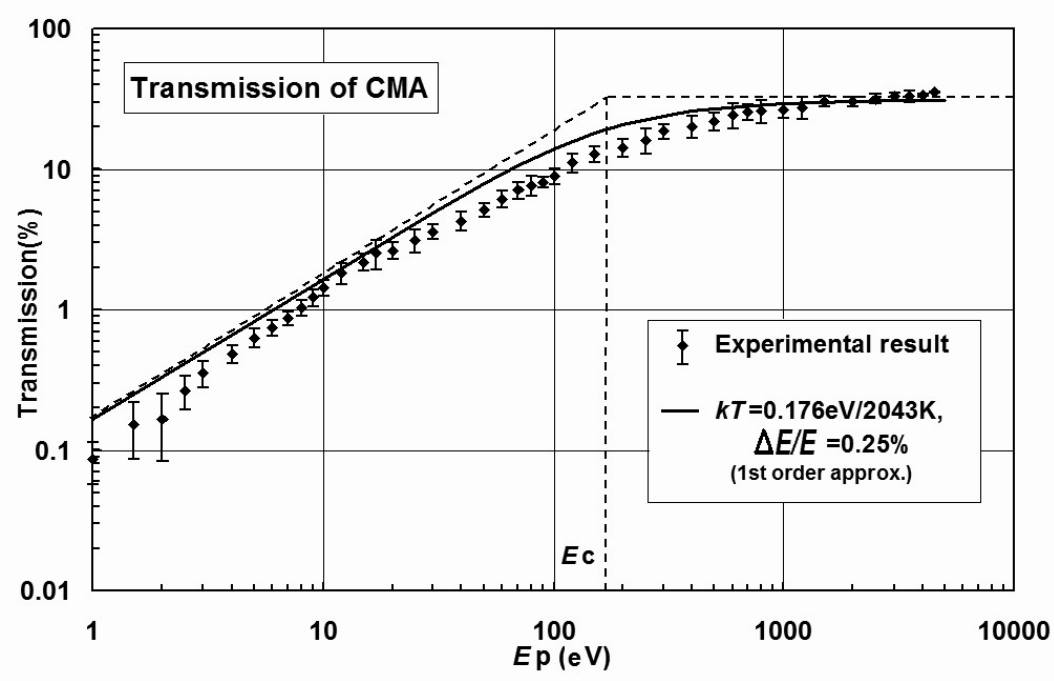

Fig. 2. Transmission of CMA experimentally obtained and fitted first order approximation (solid-line).

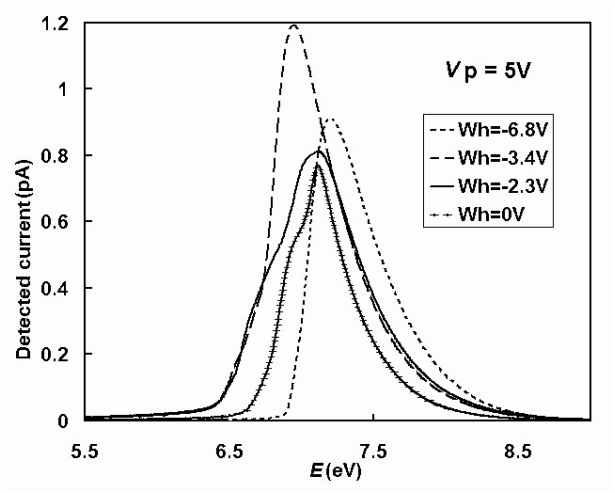

Fig. 3. Thermionic emission spectra measured by FC_2 for Wehnelt bias 0 through –6.8 V (V_p=5 V).

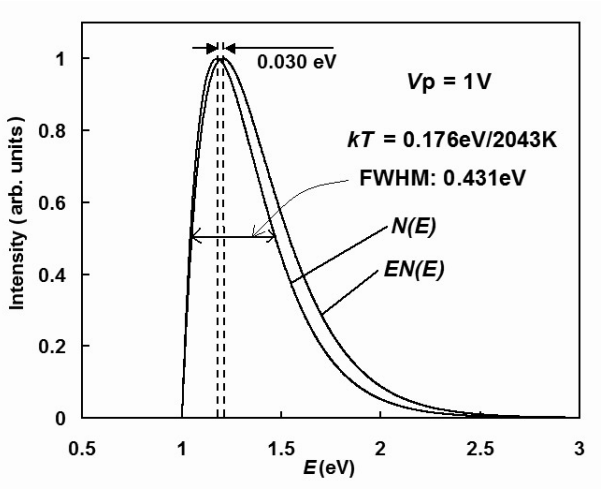

Fig. 5. $EN(E)$ and $N(E)$ characteristics for thermionic emission (kT=0.176 eV/2043 K) at V_p=1 V.

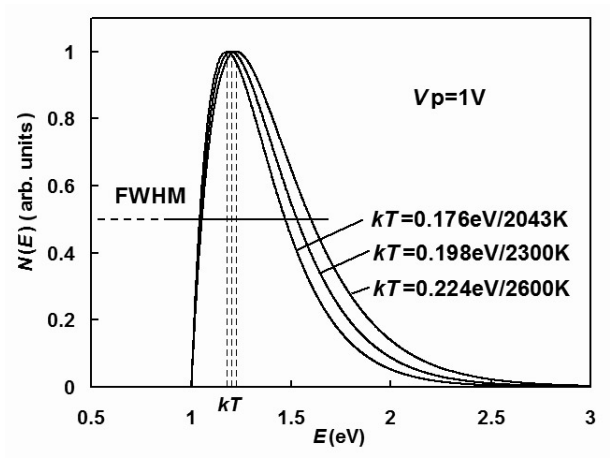

Fig. 4. Energy distributions of thermionic emission for kT of 0.176, 0.198, and 0.224 eV for the acceleration of V_p=1 V.

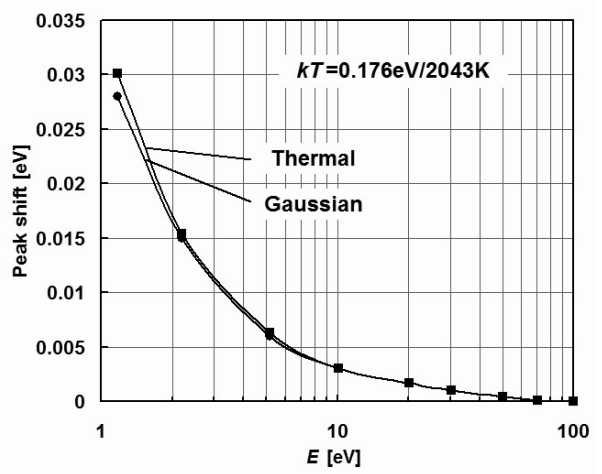

Fig. 6. Thermionic and Gaussian peak shifts from the original sources due to $EN(E)$ characteristics for kT=0.176 eV/2043 K and the peak at 0.176 eV, respectively.

acceleration voltage V_p=1 V. Such a low voltage may be meaningless in AES but for the emphasis of the feature. In the general case the emitted electron peak is assumed to be Gaussian. The half width of the peak is FWHM 2.3548σ [17], σ being the standard deviation. To compare the results with those of thermionic emission, the standard deviation of the Gaussian distribution was assessed so that the FWHM to be the same as for the thermionic emission, then we have a relation, σ=1.043kT.

Since CMA provides $EN(E)$ not $N(E)$ shown in Fig. 4, the energy distribution to be measured with CMA, $EN(E)$, is compared with $N(E)$ in Fig. 5, where a slight shift of the peak position is predicted for both cases, thermionic emission and Gaussian distributions. For the other energies up to 100 eV, the shift is shown in Fig. 6. We noticed that in both cases, particularly in the lower energies, the peak position shifts due to the "amplification" factor E were pronounced and it decreased quickly with energies. The FWHM in the corresponding spectra increase as well. It seems, however, the shape of the thermionic peak was affected by this factor for the higher energies, whereas that in the symmetric Gaussian peak was almost only the whole shift. For higher energy range (>0.1E_c), spectrum changes due to the convolution were significant. In the thermionic peak, peak position was shifted toward higher energy, whereas in the symmetric Gaussian peak no shift has occurred.

3.3. Simulation results

3.3.1. Peak intensity

The convolution results are shown in Fig. 7, in which the peak intensities for three combinations were presented. i.e., 1. Gaussian spectra (G) through Gaussian resolution function (G), 2. G through the triangle resolution function (TGL), and 3. thermionic emission (TH) through TGL. In the convolution, the thermal energy kT was of 0.176 eV/2043 K and thus FWHM 0.431 eV. The same value of FWHM was applied to G. The energy resolution $\Delta E/E$ was 0.25% in common. This graph was compared with the experimental results after been adjusted to the measured value in the high energy E_p 31% (Fig. 2). The corner energy (E_c) was found at about 180 eV. This was a good approximation of experiments already mentioned in Fig. 2. The characteristics almost coincided in the higher and lower ranges as first approximation. At corner energy Ec, the curve G-G revealed $1/\sqrt{2}$ of the saturated level (that in higher energies). While the curves G-TGL and TH-TGL revealed about 5 and 12% lower values than G-G. Every case, however, could be represented as the same common corner energy E_c. This fact may be convenient to assess any spectra and analyzer.

The other combinations of Th-TGL (Fig. 8) are identical (by the shift of the E_c) these curves can be expressed in a universal curve so called first order response. Slight energy shift and broadening of the spectrum can simultaneously be occurred and discussed in the followings.

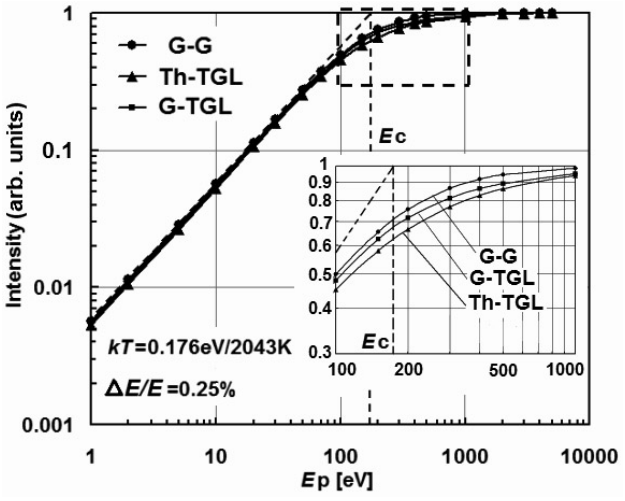

Fig. 7. Peak intensity by convolution simulation for the Gaussian (G) and thermionic emission (Th) spectra being analyzed with energy resolution functions (0.25%) of Gaussian (G) and triangle (TGL). The corner energy E_c is 180 eV. Inset is a detail around the corner energy.

3.3.2. Peak position

The result of convolution for other accelerations higher than 10 V are shown in Fig. 9 for thermal energies, kT=0.176 (a), 0.198 (b), and 0.224 eV (c) and resolution functions of 0.2, 0.25, 0.4, and 0.6% as parameters. Apparent peak position is plotted as a function of the primary energy E_p. Broken line showing a level of kT indicates the original peak position. The characteristics would saturate at higher energies, which seems as the

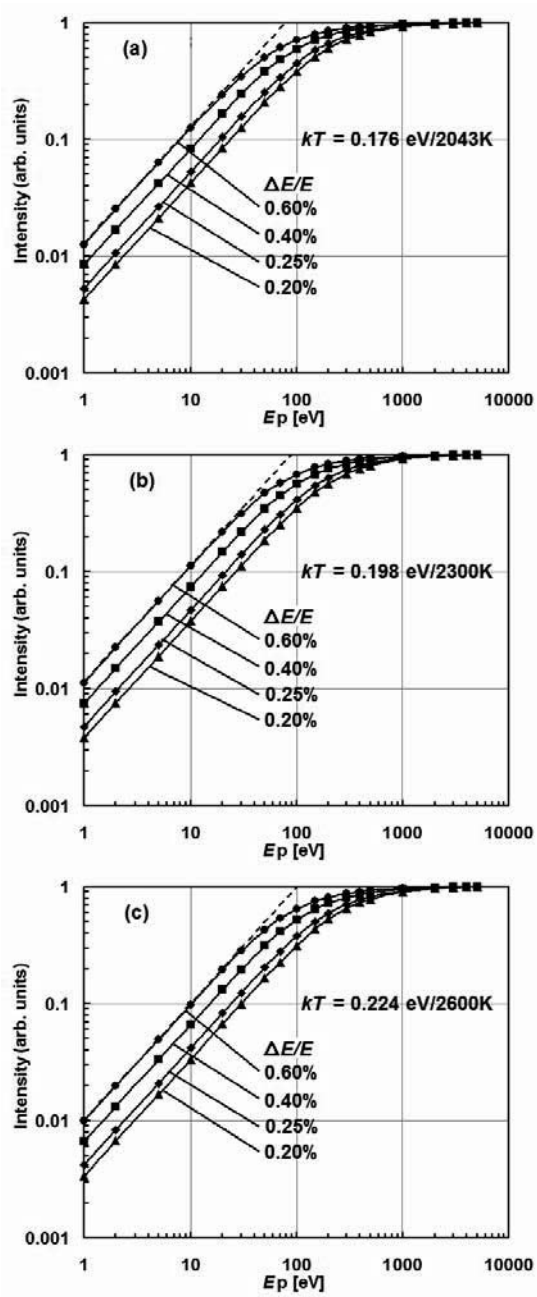

Fig. 8. Calculated peak Intensity for thermionic emissions; kT=0.176 (a), 0.198 (b), and 0.224 eV (c). The parameters are energy resolutions for the triangle functions; 0.2, 0.25, 0.4, and 0.6%.

corner energy E_c. The ratio of the saturated levels to those originals was about 1.68 irrespective of the thermal energies. The bends in the lower energies below 10 eV were caused by the $EN(E)$ characteristics already mentioned in section 3.2.

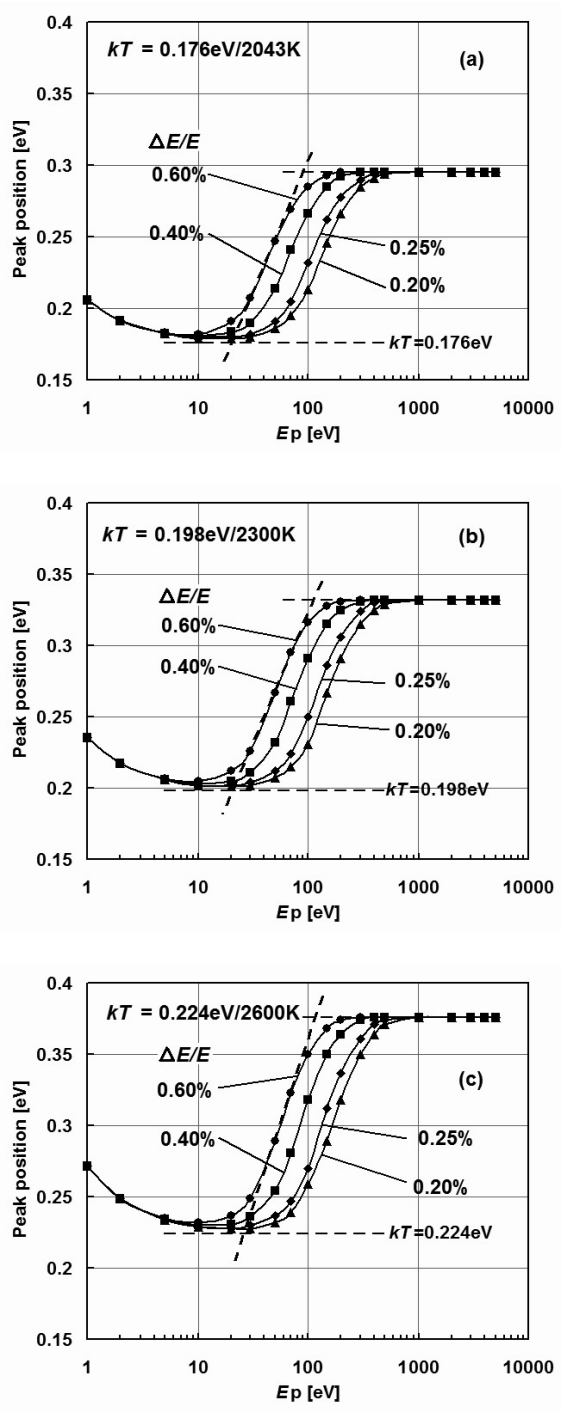

Fig. 9. Calculated peak position for thermal energies; kT=0.176 (a), 0.198 (b), and 0.224 eV (c). The parameters are energy resolutions; 0.2, 0.25, 0.4, and 0.6%. Dashed lines are peak positions of the original spectra.

3.3.3. Peak width (FWHM)

The convolution simultaneously illustrated the change of spectrum peak width in FWHM. Figure 10 is one example for three combinations of spectra and resolution functions that same as in Fig. 7. This characteristic also showed the corner energy E_W at the cross section of the extrapolation of the curve from the lower and higher energies. The characteristic seemed another first order response with the corner energy at E_W, which was also similar or identical value as E_c. The flat region in the lower energies was of the inherent spectrum peak width. The slight increased value around 1 eV was due to $EN(E)$ characteristic mentioned in 3.2. The other combinations of thermionic emissions [kT= 0.176 (a), 0.198 (b), and 0.224 eV (c)] and energy resolution functions (0.2, 0.25, 0.4, and 0.6%) are depicted in Fig. 11. All those curves can be expressed only one parameter of the corner energy E_W, which is almost the corner energy E_c.

4. Conclusion

The transmission characteristics of our CMA were measured using a mini-electron gun representing the sample. Down to electron energies of several eV, the transmission determined is similar to that expected from the theory of CMA. The obtained results were almost identical with the optical transmission measurement for the meshes used. The optical transmission can be estimated by calculation so that our CMA is in a calculable category. Our simulation allows analyzing the depend-

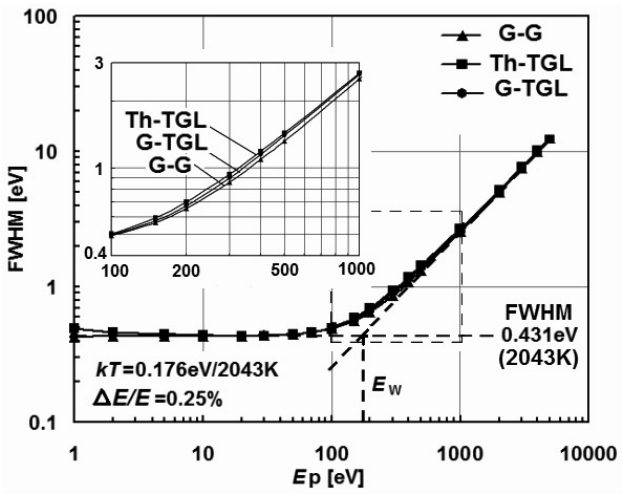

Fig. 10. Spectrum peak width in FWHM for thermionic emission and Gaussian spectra as in Fig. 7.

ence of the characteristics on certain parameters in a way difficult to do experimentally.

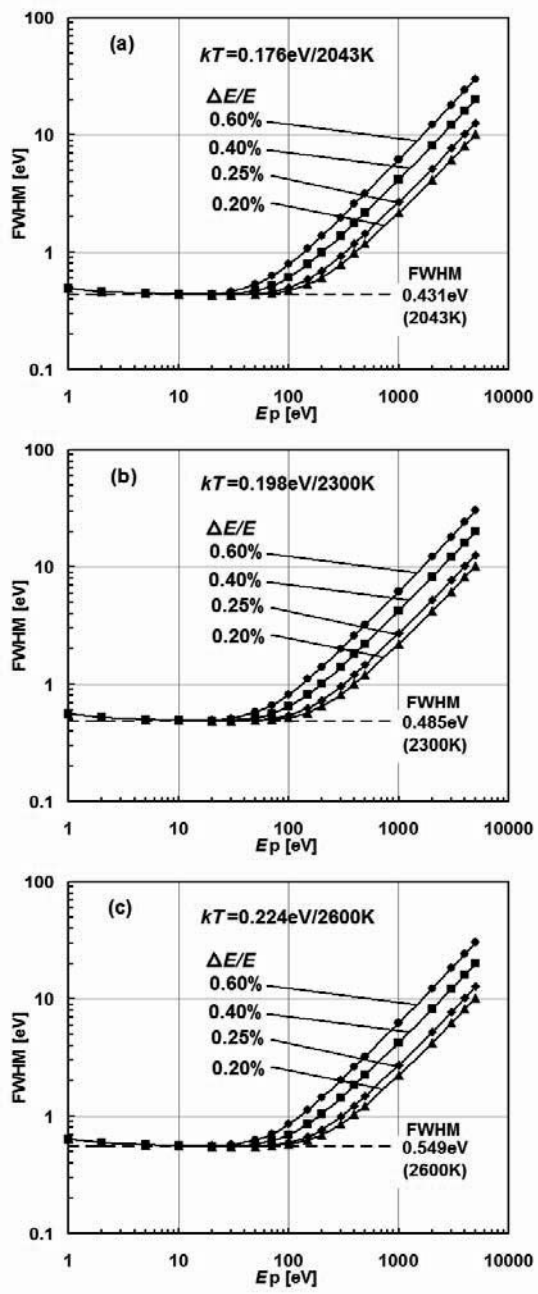

Fig. 11. Calculated peak width for thermal energies; kT=0.176 (a), 0.198 (b), and 0.224 eV (c) Parameters are energy resolutions 0.2, 0.25, 0.4, and 0.6%. Dashed lined are the levels of original spectra.

5. Acknowledgements

The Special Coordinated Research of Science and Technology through NIMS have supported the work. We would like to express our gratitude for the members of Surface Analysis Society of Japan for their helpful comments and appreciated encouragements for this work. Dr. S. Ichimura, Dr. Y. Yamauchi and Ms Y. Shoji in AIST encouraged K.G. to perform the work. One of the authors (A.A.) would like to express his gratitude to the Japanese Ministry of Education, Culture, Sports, Science and Technology for the scholarship.

6. References

[1] *Handbook of Auger Electron Spectroscopy*, Physical Electronics Industries, Eden Prairie, MN, (1976).

[2] *Auger Electron Spectra Catalogue*, ANELVA Corporation, (1979).

[3] *Handbook of Auger Electron Spectroscopy*, JEOL, (1982).

[4] M. P. Seah, *J. Electron Spectrosc. Relat. Phenom.* **97**, 235 (1998).

[5] G. C. Smith and M. P. Seah, *Surf. Interface Anal.* **16**, 144 (1990).

[6] M. P. Seah, *J. Electron Spectrosc. Relat. Phenom.* **71**, 191 (1995).

[7] C. J. Powell, N. E. Erickson, and T. E. Madey, *J. Electron Spectrosc. Relat. Phenom.* **25**, 87 (1982).

[8] C. J. Powell and M. P. Seah, *J. Vac. Sci. Technol. A* **8**, 735 (1990).

[9] M. P. Seah and G. C. Smith, *Surf. Interface Anal.* **17**, 855 (1991).

[10] *Calibration, in Philosophy in Practice*, 2nd Ed., 3-3~3-7, John Fluke (1996).

[11] K. Goto, *J. Surf. Anal.* **9**, 18 (2002).

[12] K. Goto, N. Sakakibara, and Y. Sakai, *Microbeam Anal.* **2**, 123 (1993).

[13] K. Goto, N. Sakakibara, and Y. Takeichi, Y. Numata, and Y. Sakai, *Surf. Interface Anal.* **22**, 75 (1994).

[14] http://www.sasj.jp/COMPRO/index.html.

[15] W. Y. Li, A. A. Iburahim, K. Goto, and R. Shimizu, *J. Surf. Anal.* **12**, 109 (2005).